

Structural Basis for Targeting of Human RNA Helicase DDX3 by Poxvirus Protein K7

Shun-ichiro Oda,¹ Martina Schröder,² and Amir R. Khan^{1,*}

¹School of Biochemistry and Immunology, Trinity College, Dublin, Dublin 2, Ireland

²Institute of Immunology, National University of Ireland, Maynooth, County Kildare, Ireland

*Correspondence: amirrafk@tcd.ie

DOI 10.1016/j.str.2009.09.005

SUMMARY

Poxviruses are DNA viruses that express numerous proteins to subvert the host immune response. Vaccinia virus protein K7 adopts a Bcl-2 fold and displays structural and functional similarities to Toll-like receptor antagonist A52. Both proteins interact with IRAK2 and TRAF6 and suppress TLR-dependent NF- κ B activation. However, unlike A52, K7 also forms a complex with RNA helicase DDX3 and antagonizes interferon- β promoter induction. We have narrowed the K7 binding site to an N-terminal peptide motif of DDX3 ahead of its core RNA-helicase domains. The crystal structure of full-length K7 in complex with the DDX3 peptide reveals a thumblike projection of tandem phenylalanine residues of DDX3 into a deep hydrophobic cleft. Mutagenesis of these phenylalanines abolishes the effects of DDX3 on interferon- β promoter induction. The structure of K7-DDX3 reveals a novel binding mode by a viral Bcl-2 protein that antagonizes a key pathway in innate immunity.

INTRODUCTION

The innate immune system is critical for the detection of invading pathogens and generation of the early inflammatory response. Pattern recognition receptors (PRRs), such as Toll-like/interleukin-1 receptors (TLRs) and RIG-like helicases (RLHs), recognize distinct molecular patterns on viruses and bacteria (O'Neill, 2006; Takaoka and Taniguchi, 2008). TLR and RLH engagement results in complex downstream signaling cascades involving adaptor proteins and kinases, ultimately leading to activation of the transcription factors NF- κ B and interferon regulatory factors (IRFs) 3 and 7. This activation subsequently leads to the release of proinflammatory cytokines and type I interferons (Moynagh, 2005). Stimulation of TLR3, TLR4, and RLH leads to downstream activation of the kinases TBK1 and IKK ϵ , which is essential for activation of IRF3/IRF7 and subsequent interferon β (IFN- β) promoter induction.

Poxviruses are large double-stranded DNA viruses that have evolved numerous mechanisms for evasion of innate immune signaling pathways. Vaccinia virus (VACV), the prototypical member of the *Poxviridae* family that is used for the smallpox vaccine, replicates within the cytosol of infected cells and

encodes over 200 open reading frames (Smith et al., 1991). During poxvirus infection, several viral proteins are expressed in the cytosol that antagonize the inflammatory response and favor viral replication (Bowie and Unterholzner, 2008). In particular, VACV proteins A46 and A52 were shown to specifically antagonize TLR signaling (Bowie et al., 2000; Harte et al., 2003; Maloney et al., 2005; Stack et al., 2005). The discovery of this viral evasion strategy provided early evidence for a role of TLRs in the antiviral immune response. A46 contributes to virulence by targeting multiple TLR adaptor proteins, resulting in membrane-proximal inhibition of TLR signaling and suppression of NF- κ B and IRF3 activation (Bowie and Unterholzner, 2008; Stack et al., 2005). A52 acts further downstream and inhibits NF- κ B activation by targeting IRAK2 (Harte et al., 2003; Keating et al., 2007; Maloney et al., 2005). In addition, binding of A52 to TRAF6 mediates p38 MAP kinase activation and enhances TLR-mediated activation of the anti-inflammatory cytokine IL-10 (Maloney et al., 2005).

VACV protein K7 has 20% overall sequence identities to A52. Both K7 and A52 interact with TRAF6 and IRAK2 and inhibit TLR-induced NF- κ B activation (Schröder et al., 2008). However, unlike A52, K7 binds to human DEAD-box RNA helicase DDX3 and inhibits TLR-dependent and -independent IRF3/7 activation and induction of the IFN- β promoter. The investigation of this K7-mediated viral evasion strategy led to the discovery of a novel role for DDX3 in innate immunity (Schröder et al., 2008). DDX3 binds to and is phosphorylated by IKK ϵ and/or TBK1 (Schröder et al., 2008; Soulat et al., 2008), the two kinases that are essential for IRF3/IRF7 activation. Following PRR stimulation of innate immune signaling, DDX3 enhances IRF3 activation and IFN- β induction (Schröder et al., 2008; Soulat et al., 2008). K7 binding to DDX3 interferes with the activation of IRF3/IRF7 and subsequent induction of the IFN- β promoter. DDX3 appears to have multiple cellular functions and has previously been implicated in transcriptional and translational control of gene expression, RNA splicing and export, and cell cycle control (Rosner and Rinkevich, 2007). Hepatitis B virus (HBV), hepatitis C virus (HCV), and human immunodeficiency virus (HIV) also express proteins that interact with DDX3 during their replication cycle (Ariumi et al., 2007; Kwong et al., 2005; Wang et al., 2009). The Y chromosome-encoded DDX3Y isoform is highly conserved throughout its amino acid sequence with DDX3X, the subject of this study. However, DDX3Y gene expression is restricted to male reproductive organs, where it is essential for spermatogenesis (Lardone et al., 2007).

Recent structural work has provided some insight into the molecular basis for poxvirus antagonism of innate immunity.

The crystal structures of VACV proteins A52, B14, and N1 revealed that they adopt an α -helical Bcl-2 fold. However, these proteins are devoid of sequence similarities to each other and to viral and cellular members of this superfamily (Cooray et al., 2007; Graham et al., 2008). Similarly, the NMR structure of VACV protein K7 also revealed a Bcl-2 fold, but in contrast to the other VACV proteins, K7 was found to be a monomer in solution (Kalverda et al., 2009). Viral and cellular Bcl-2 proteins regulate cell death by forming hetero-oligomers via a surface groove that binds to α -helical BH3 motifs of partner Bcl-2 proteins. The groove is formed by helices α 2– α 5 and is observed in various conformational states, ranging from “open” to “closed” in the absence of BH3 ligands (Day et al., 2005; Day et al., 2008; Kvan-sakul et al., 2007; Liu et al., 2003a; Petros et al., 2001; Sattler et al., 1997). The groove is “open” in the ligand-bound state of conventional Bcl-2 proteins that regulate apoptosis, thus enabling intimate hydrophobic contacts with amphipathic BH3 α helices (Kvansakul et al., 2007; Liu et al., 2003b; Petros et al., 2004; Sattler et al., 1997).

The structures of K7, A52, and B14 revealed a closed BH3 groove that is apparently incompatible with binding to α -helical BH3 motifs, because these three viral proteins do not regulate apoptosis (Graham et al., 2008; Schroder et al., 2008). Our previous biochemical studies showed that K7 recognizes a segment of DDX3 (residues 61–90) that is upstream of the conserved tandem RecA-like helicase domains (residues 168–576) (Kalverda et al., 2009). This region correlates with a functional role for the DDX3 N terminus (residues 1–139) in the induction of the IFN- β promoter (Schroder et al., 2008), suggesting that K7 binds to the region of DDX3 that mediates this effect. The N terminus of DDX3X (1–139), the X chromosome isoform of DDX3, is enriched in serine residues (27), glycine (20), and charged amino acids (25 Lys+Arg+His; 22 Asp+Glu). This segment of DDX3 is presumably unstructured and is not conserved in other RNA helicases or known proteins in sequence databases. This N-terminal segment was removed in the published crystal structure of DDX3, which was determined using the fragment 168–582 (Hogbom et al., 2007).

Despite the identification of numerous cellular targets of VACV proteins, there is currently little structural information regarding the protein-protein complexes formed during infection. The only structure of a poxvirus Bcl-2 protein with its target involves a BH3 peptide from Bak, which binds to the canonical BH3 groove of myxoma M11 protein (Kvansakul et al., 2007). Intriguingly, K7 and A52 share similar three-dimensional structures and common cellular targets, but A52 is unable to bind DDX3 (Schroder et al., 2008). Here, we have identified a peptide motif in the N-terminal region of DDX3, ahead of the core RNA helicase domains, that largely retains the binding affinity to K7. The crystal structure of full-length 149-residue K7 in complex with a 20-residue DDX3 peptide (residues 71–90) has been determined by single-wavelength anomalous diffraction (SAD) methods. The complex reveals the molecular basis for K7-DDX3 specificity via a binding mode that is novel within the Bcl-2 superfamily. We identify key residues that mediate the interaction between DDX3 and K7 and demonstrate that a tandem phenylalanine motif in DDX3 that is sequestered by K7 is also required for IRF3 activation and IFN- β promoter induction.

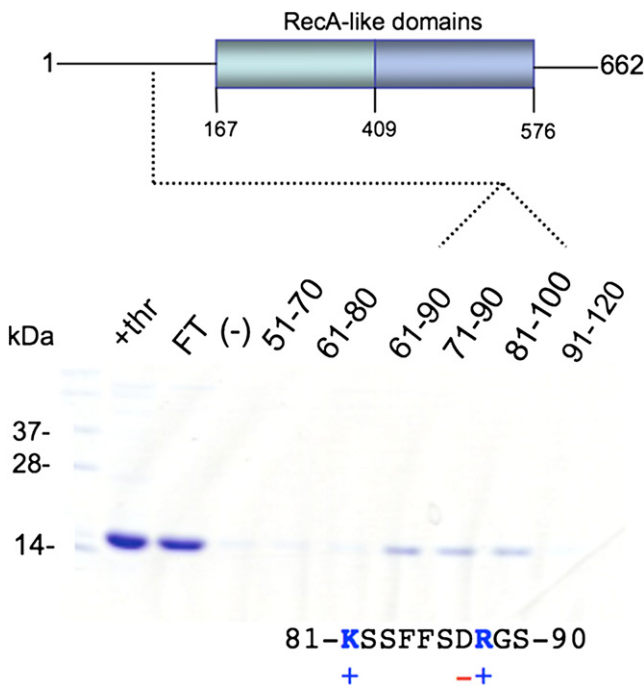


Figure 1. Biochemical Mapping of the Interaction Between K7 and DDX3

Previous work had mapped the K7-interacting region to residues 61–90 of DDX3. Smaller overlapping His-tagged peptides were used to pull down untagged K7 and visualize the protein by Coomassie blue stain. The lane marked “+thr” denotes K7 treated with thrombin, which migrates at 16 kDa. This protein was subjected to further purification by a second Ni²⁺-agarose column (lane FT). In the negative control lane (-), Ni²⁺, but not peptide, was added to K7. Only those His-tagged peptides spanning the region 81–90 of DDX3 were able to pull down K7. The sequence of this region of DDX3 is shown for convenience. The peptides are approximately 2–3 kDa in size and are too small to be visualized in these SDS-PAGE gels.

RESULTS

K7-Interacting Region of DDX3

The N-terminal region of DDX3 (1–167) was presumed to be unstructured, and a circular dichroism (CD) analysis supports this prediction (see Figure S1 available online). Previous truncations of DDX3 had minimized the K7-binding region to 30 residues (61–90) (Kalverda et al., 2009). The interacting region was further narrowed using a series of overlapping DDX3 peptides (Figure 1). All peptides were synthesized with a hexahistidine-tag at the N terminus to facilitate a pull-down assay with purified, untagged K7. The results indicate that DDX3 segment 81–90 is necessary for binding to K7 (Figure 1). Isothermal titration calorimetry experiments confirmed that DDX3 peptides encompassing the segment 81–90 largely retained the affinity of a nearly complete fragment of DDX3 (5–580) that included the N terminus and the two RecA-like domains (Figure 2). Consequently, peptides 61–90, 71–90, and 81–100 lacking the hexahistidine tag were synthesized, because these were deemed suitable for cocrystallization with K7. The best crystals were obtained with peptide 71–90, and, following selenomethionine derivitization of K7, the crystal structure of K7-DDX3 was solved by SAD methods.

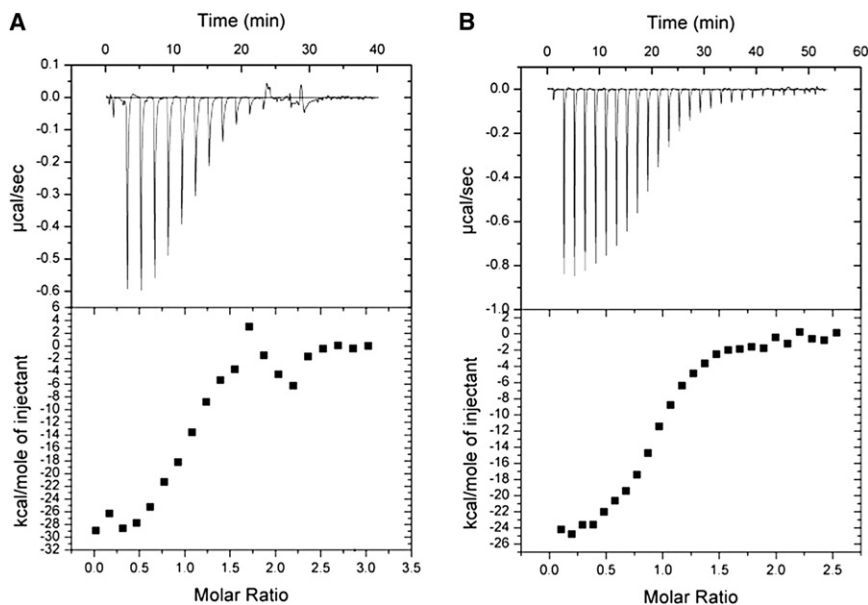


Figure 2. Isothermal Titration Calorimetry of K7-DDX3 Complex Formation

(A) Full-length K7 (400 μM) was injected into DDX3₅₋₅₈₀ (30 mM) in the sample cell. (B) DDX3 peptide 71-90 (250 μM) was injected into the cell containing full-length K7 (30 μM). Data were fit using Origin software version 7.0. The K_d was 510 nM for the fragment 5-580 and was modestly weaker for the peptide 71-90 (930 nM), demonstrating that this peptide largely retains its affinity to K7. The stoichiometry deduced from data fitting is close to 1 for both titrations shown. The thermodynamic parameters are summarized in Table 1.

Structure of K7

The final model of K7-DDX3 was refined using data to 1.6 Å and includes residues 6-149 of K7, 82-88 of DDX3, and 261

First, K7 is a monomer, whereas the other VACV proteins—A52, B14, and N1—are dimers (Aoyagi et al., 2007; Cooray et al., 2007; Graham et al., 2008; Kalverda et al., 2009). As

water molecules (Figures 3 and 4). Consistent with the uncomplexed NMR structure, K7 adopts an α-helical topology belonging to the Bcl-2 family that consists of a core of seven α helices. However, K7 is a noncanonical member of the Bcl-2 family in several respects.

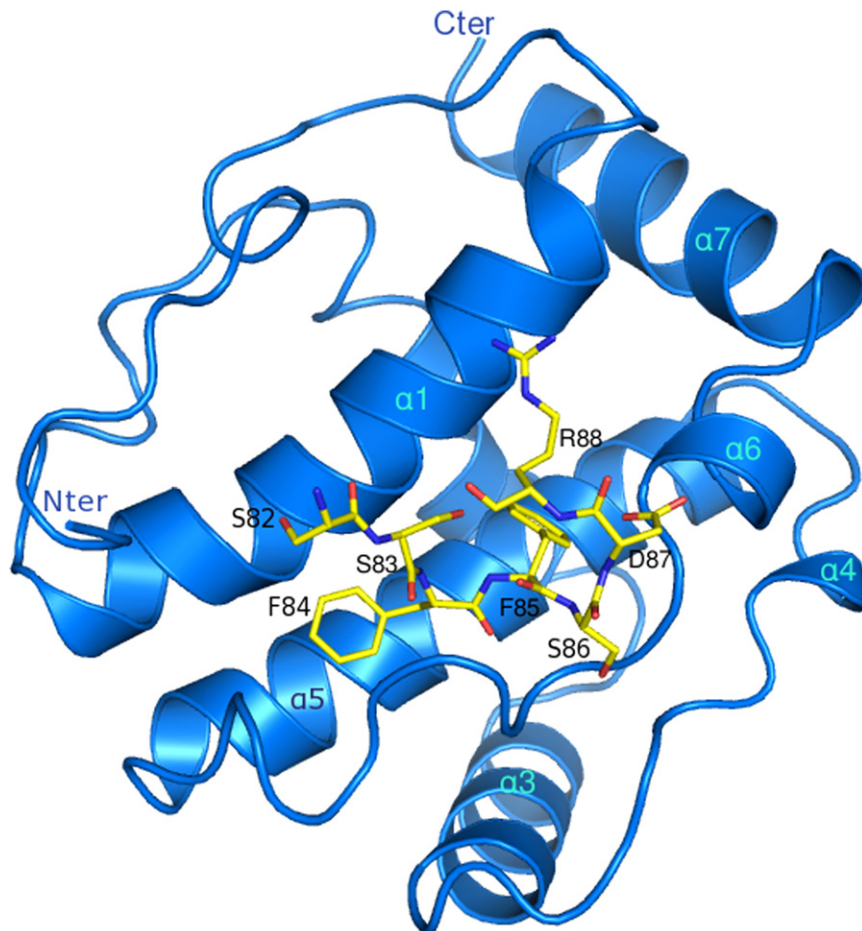


Figure 3. Structure of K7-DDX3 Complex

K7 is shown in blue ribbons, and the peptide 82-88 is a yellow stick model. Canonical Bcl-2 family nomenclature is used for α helices, although K7 lacks α4 and α6.

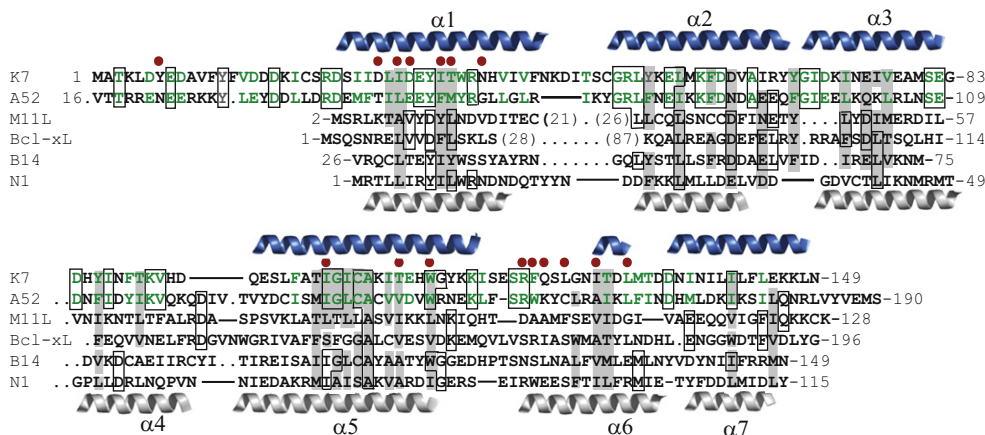


Figure 4. Structure-Based Sequence Alignment of Poxvirus Bcl-2 Proteins

Structures were aligned using a secondary structure matching algorithm in COOT (Emsley and Cowtan, 2004), and the alignment was manually adjusted where necessary. Green residues are conserved between K7 and A52. The gray shading indicates conservation of the hydrophobic core in the Bcl-2 family, despite the absence of sequence identities. Red dots mark DDX3-interacting residues of K7.

a consequence, an additional surface is exposed in K7 that is critical for DDX3 binding (see below). Second, two of the seven canonical α helices ($\alpha 4$ and $\alpha 6$) are nonhelical in K7. The atypical conformation of these two segments of K7 is necessary to form a deep hydrophobic pocket to accommodate the DDX3 peptide. Third, the canonical groove that binds to BH3 domains of cellular proapoptotic Bcl-2 proteins is closed in K7. Unlike conventional Bcl-2 homologs, K7 does not antagonize innate cell death pathways. In this latter respect, K7 resembles VACV proteins A52 and B14, whose crystal structures were recently determined (Graham et al., 2008). K7 and A52 share 27% sequence identities (54% homology) within their core Bcl-2 domain, and both proteins have a closed BH3 groove. Upon superposition of K7 and A52 secondary structures, the root-mean-square (rms) deviation (rmsd) of 108 aligned C_{α} atoms is 1.89 Å. Apart from A52, the closest structural relative of K7 is VACV protein N1 (PDB code 2i39; 2.0 Å rmsd over 96 residues). N1 is a conventional antiapoptotic protein with an open BH3 groove that interacts with cellular Bcl-2 proteins Bad, Bax, and Bid (Cooray et al., 2007). K7 and A52 are devoid of significant sequence identities to N1, B14, and other viral and cellular Bcl-2 proteins (Figure 5).

Nevertheless, K7, A52, and B14 share a Bcl-2 scaffold with a closed BH3 groove and antagonize distinct immune signaling pathways.

Structure of the K7-DDX3 Complex

The DDX3 peptide binds to a negatively charged face of K7 and protrudes into a deep hydrophobic pocket (Figures 4–6). Residues 82–88 of DDX3 are ordered in both molecules of the asymmetric unit and have an identical conformation. The bound DDX3 peptide segment is entirely consistent with our in vitro pull-down assays and thermodynamic studies. The hydrophobic binding pocket in K7 is bordered by the N terminus (Tyr7), $\alpha 1$, and the region 118–127, which is predominantly nonhelical but is labeled “ $\alpha 6$ ” to remain consistent with the canonical Bcl-2 fold. Despite lacking secondary structure, the backbone in this segment is well ordered in electron density maps. A52, which is the closest relative of K7, is α -helical ($\alpha 6$) in this corresponding segment (residues 154–168; Figures 4 and 7). Strikingly, the dimeric interface of A52 comprises $\alpha 1$, $\alpha 6$, and the N terminus, which maps directly onto the DDX3-binding site of K7. All of the known VACV Bcl-2-family proteins are homodimers, and the dimeric

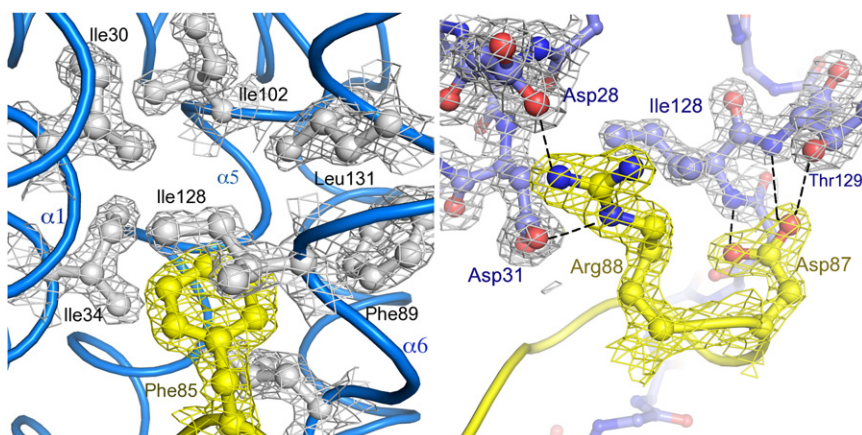


Figure 5. Refined Electron Density of the K7-DDX3 Complex

The map ($2F_o - F_c$) was calculated using all atoms and is contoured at 1.5 σ . The electron density around the peptide is colored yellow to distinguish it from K7, using the program Pymol.

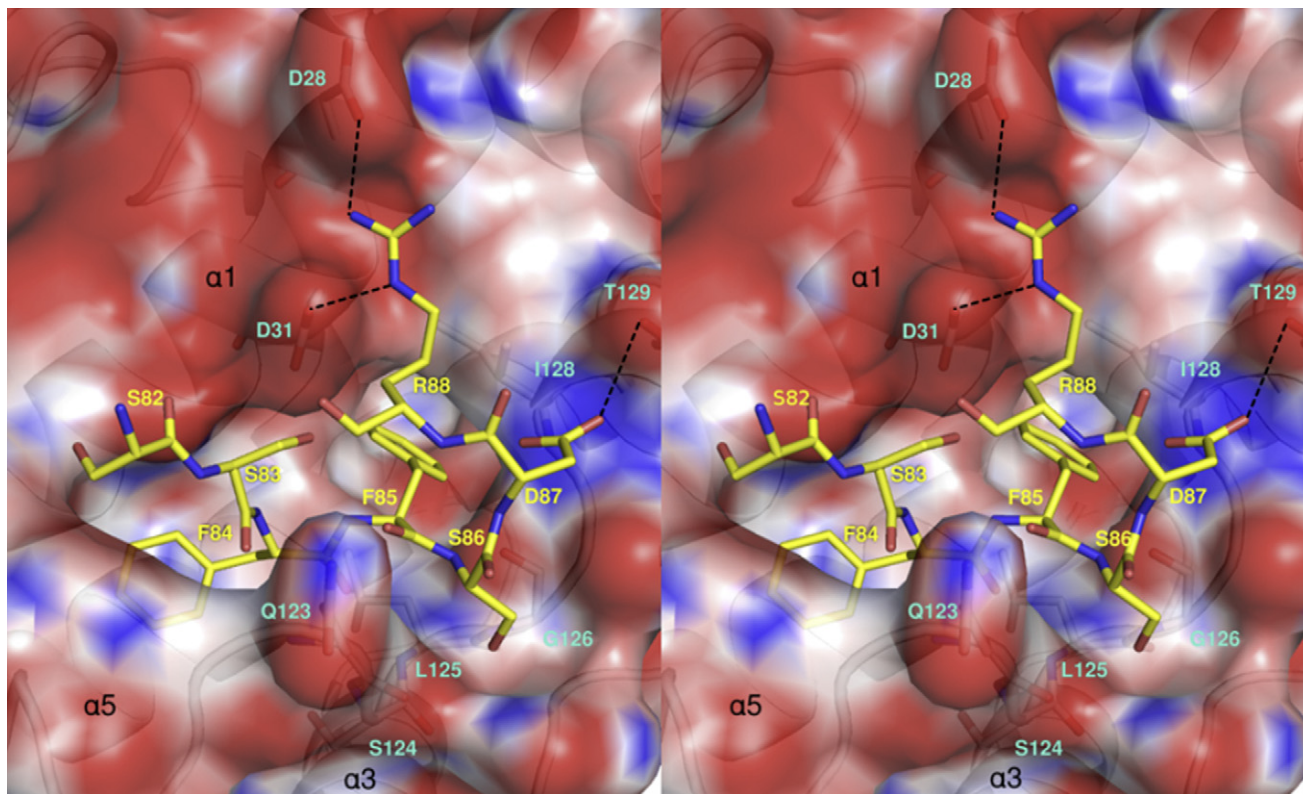


Figure 6. Electrostatic Surface View of K7 in Divergent Stereo

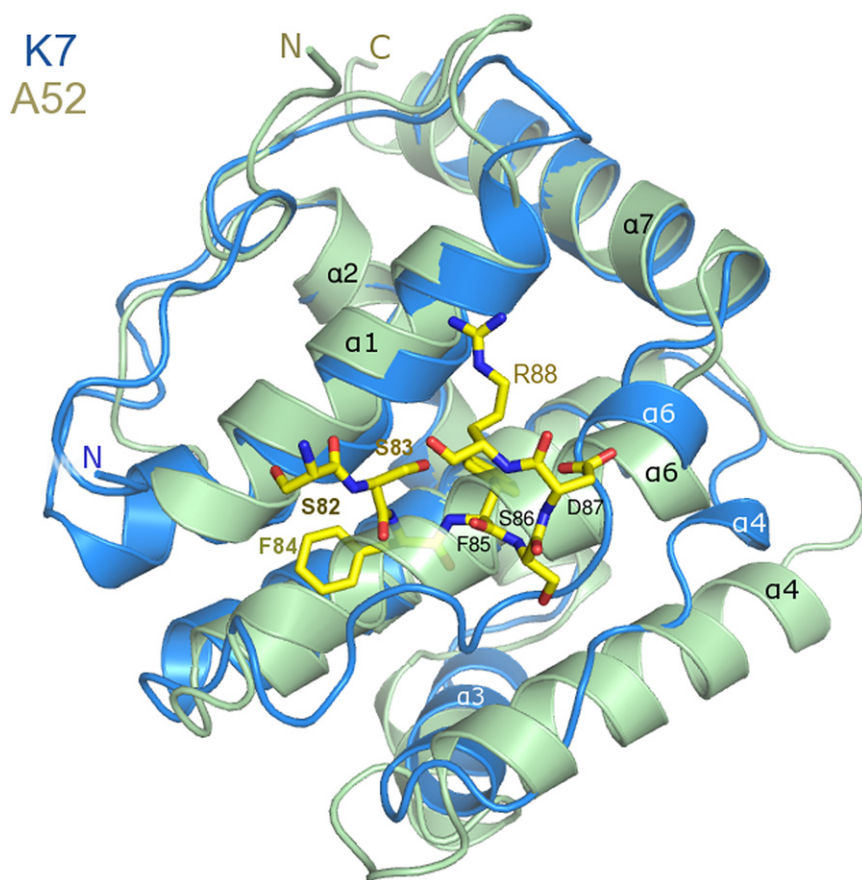
The peptide is represented as a stick model. Stereo rendering reveals the depth of penetration by Phe85 into the K7 pocket.

interface is broadly conserved in the superfamily (Graham et al., 2008). In contrast, K7 is a monomer, and this face is therefore free to interact with DDX3. Furthermore, this face of K7 has a predominantly negatively charged character that is complementary to positively charged DDX3. The overall pI of K7 is 4.8, whereas the N-terminal segment of DDX3 (1–143) preceding the α -helical “flanking region” (residues 144–167) and core helix domains has a pI of 7.8 (Hogbom et al., 2007; Sengoku et al., 2006).

The conformation of the bound peptide begins with an extended segment (Ser82–Ser83), followed by a loop that is anchored at the tip by two phenylalanine side chains, Phe84 and Phe85. Strikingly, the insertion of these aromatic residues into a deep hydrophobic cleft effectively means that the DDX3 peptide occupies the position of $\alpha 6$ in the canonical Bcl-2 fold. The intimate association of K7-DDX3 is reflected in hydrogen bonds between the side chain of Asp87 and the backbone amides of Ile128 and Thr129, which nucleate a single turn α helix ($\alpha 6$). Asp87 also forms a hydrogen bond with the side chain of Thr129, further stabilizing the conformation of K7 at the N terminus of $\alpha 6$. The peptide conformation is stabilized by two internal hydrogen bonds. The first involves Ser83(O γ) and the backbone amide of Phe85. The second internal hydrogen bond (3.4 Å) comprises the backbone of Phe85(CO) and the backbone amide of Arg88 that is reminiscent of an α -helical 3_{10} hydrogen bond. The N and C termini of the peptide approach close in space such that the α -carbon atoms of Ser82 and Arg88

are within 6 Å. Thus, the overall peptide adopts a thumblike projection into a hydrophobic pocket of K7. The peptide is likely disordered in solution, as evidenced by CD spectroscopy of the fragment 5–167 of DDX3 (Figure S1). Furthermore, a second K7-binding site for the peptide reveals a completely different conformation for the diphenyl motif. This second site is situated on the surface of molecule B in the asymmetric unit and mediates crystal contacts along the layer aligned with the AC face of the monoclinic lattice (Figure S2). Although this second site is not biologically relevant, the variable conformation of the peptide adopted during crystallization suggests significant flexibility in solution, prior to complex formation with K7.

Interactions between K7 and the DDX3 peptide involve hydrophobic contacts, hydrogen bonds, and electrostatic interactions. The packing of the diphenyl motif of DDX3 completes the central piece of a continuous stretch of K7 aromatic residues comprising Phe43, Tyr7, Phe122, and Phe89. The key determinant of electrostatic complementarity is Arg88 of DDX3, which forms salt bridges to both Asp28 and Asp31 (O $\delta 2$). Asp31 (O $\delta 1$) is also hydrogen bonded to DDX3 residue Ser83 (O γ). A total of 545 Å² of K7 is buried in the complex, whereas 126 Å² (30% of total surface area) of the DDX3 peptide becomes buried after complex formation. Superposition of the uncomplexed NMR structure of K7 with the bound complex reveals significant flexibility around the DDX3 pocket (Figure S3). The N terminus of K7 is disordered and points away from the DDX3 pocket ($\alpha 5/\alpha 6$) in the NMR models. However, the N terminus shifts toward the

**Figure 7. Superposition of K7 and A52**

The DDX3 peptide (stick) occupies the position of $\alpha 6$ in the Bcl-2 family. A52 dimerization is mediated by its N terminus, $\alpha 1$ and $\alpha 6$, which maps onto the DDX3 binding site of K7.

DDX3 pocket in the complex, as evidenced by van der Waals contacts between Tyr7 (K7), Phe84 (DDX3), and Phe122 (K7). Overall, the monomeric state of K7 and its conformational flexibility enables the binding of DDX3 into a deep pocket. A cartoon depiction of DDX3 contacts with K7 is shown in Figure S4.

Mutagenesis of DDX3 and Immune Signaling

The structure of the K7-DDX3 complex implied that the diphenylalanine motif of DDX3, Phe84, and Phe85 is critical for the interaction with K7. These two phenylalanines were mutated to alanine to test whether this would disrupt the interaction between DDX3 and K7. Full-length myc-tagged DDX3 (662 residues) harboring two mutations, F84A+F85A (FFAA mutant), was cotransfected with Ha-tagged K7 into HEK293 cells, and immunoprecipitation experiments were performed. K7 failed to coimmunoprecipitate with the FFAA mutant (Figure 8a, lane 6), while in the same experiment it clearly coimmunoprecipitated with wild-type DDX3 (Figure 8a, lane 3). These cellular assays are consistent with *in vitro* thermodynamic studies in which the FFAA mutant peptide (71–90) of DDX3 failed to demonstrate measurable affinity with K7 by isothermal titration calorimetry (Table 1).

After having identified residues Phe84 and Phe85 as being essential for K7-DDX3 recognition, the functional relevance of the diphenylalanine motif of DDX3 in the antiviral response was investigated by immune signaling studies. In reporter-based assays, the FFAA mutant failed to enhance IRF3 activation and

IFN- β promoter induction, whereas wild-type DDX3 enhanced IKK ϵ -induced signals, as described elsewhere (Schroder et al., 2008) (Figure 8b). Altogether, our structural and functional work suggests a critical role for the diphenylalanine motif of DDX3 in IRF3 activation and type I interferon induction. In addition, these studies suggest that K7 binding to a short DDX3 segment encompassing the diphenylalanine motif is sufficient to prevent DDX3 from executing its role in innate immune signaling.

DISCUSSION

The K7-DDX3 complex represents a unique binding mode within the superfamily of Bcl-2 proteins. In effect, DDX3 occupies the position of the canonical helix $\alpha 6$ and interacts with the hydrophobic interior of K7. Hydrophobic contacts (3.6 Å) between Phe85 (DDX3) and Trp112 (K7 and $\alpha 5$) are indicative of the

depth of penetration by the diphenylalanine motif into the globular core of K7. The NMR structure of K7 revealed considerable flexibility in the region 118–127, which is an α helix ($\alpha 6$) in all other known viral and cellular Bcl-2 proteins. Furthermore, the DDX3-binding face of K7 overlaps with the dimerization interface of A52, its closest structural and functional relative. These data support a model in which monomeric K7 has evolved as a conformational trap for DDX3, guided by electrostatic complementarity and anchored by the diphenylalanine motif in its hydrophobic core. The high density of negative charges on this face likely serves the dual function of DDX3 binding, as well as contributing to the monomeric state of K7 via electrostatic repulsions. Several Asp and Glu residues on this face of K7 (Asp28, Glu119, Asp130, and Asp134) are not conserved in A52. The structure therefore explains the specific binding of K7, but not A52, to DDX3. We would also predict that none of the other described dimeric Bcl-2-like VACV proteins interact with DDX3. Despite clearly possessing Bcl-2 topology, it is not evident why $\alpha 4$ and $\alpha 6$ of K7 are largely devoid of α -helical content. It is particularly striking that 8 of 15 residues in $\alpha 4$ are identical in A52 and K7, with conservative changes in an additional four residues. Given that K7 and A52 share some cellular binding partners, such as TRAF6 and IRAK2, these proteins presumably have common epitopes elsewhere. Apart from a study showing that an A52 peptide derived from the $\alpha 4$ - $\alpha 5$ loop inhibits NF- κ B in isolation (McCoy et al., 2005), there is a lack of structural and biochemical information regarding the IRAK2 and TRAF6 binding sites.

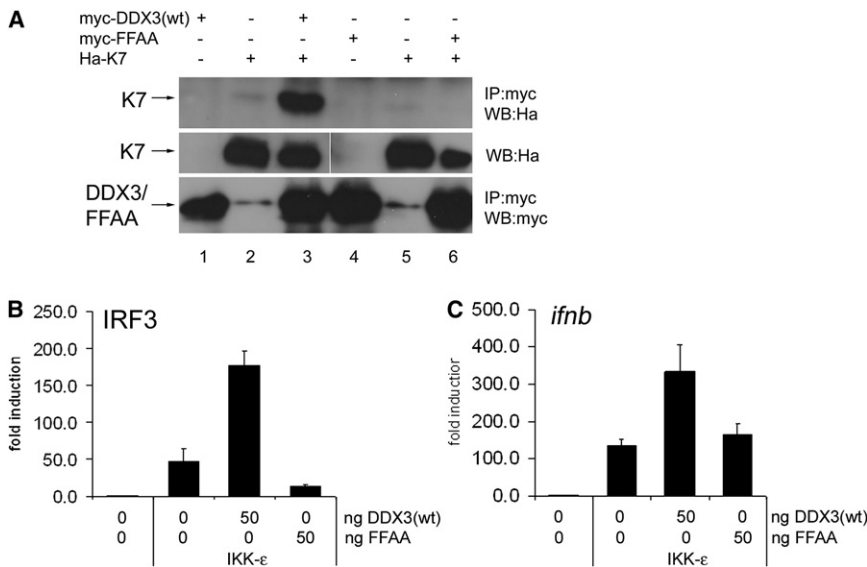


Figure 8. Phe84 and Phe85 Are Required for the Effect of DDX3 on the IRF Pathway

(A) HEK293T cells were transfected with Myc-DDX3(wild-type) or myc-FFAA mutant together with Ha-K7 for 48 hr, and the cell lysates were subjected to immunoprecipitation (IP) with the indicated antibodies. The precipitated complexes were analyzed by SDS-PAGE and Western blotting (WB) with the indicated antibodies. One representative experiment out of two is shown.

(B and C) HEK293 cells were transfected with the indicated amount (nanograms) of pCMV-DDX3 or pCMV-FFAA, 25 ng of IKK ϵ expression plasmid, and either the IRF3-GAL4 fusion protein in conjunction with a GAL4-dependent promoter or the IFN- β promoter reporter gene. A constitutively active *Renilla* luciferase construct was cotransfected to control for transfection efficiency. Luciferase activity was measured 36 hr after transfection. Data are expressed as the mean fold induction \pm SD relative to control levels, for an individual experiment performed in triplicate. The first lane in (b) and (c) is a transfection with an empty

vector (no IKK ϵ expression) that is normalized to control (basal) levels of transcription. A representative of at least three independent experiments is shown. Data are shown as the mean fold induction \pm SD relative to control levels, for an individual experiment performed in triplicate.

The recent determination of structures of three viral proteins (K7, A52, and B14) that apparently fail to bind BH3 domains allows for their comparison to canonical Bcl-2 family members. The common structural element appears to be closure of the groove on the C-terminal side of the BH3 helix binding site (Figure S5). This is due to the orientation of α 2, which is closer to α 5 in these three “non-BH3-binding” proteins. The beginning of α 5 contains the “NWGR” signature (BH1) motif of cellular Bcl-2 proteins, which is lacking in the viral homologs. VACV protein N1—which binds to the BH3 domains of Bid, Bad, and Bax—adopts an α 2 orientation similar to that of K7, A52, and B14, but it is one helical turn shorter (Figure 4), thus leaving this end of the BH3 groove open. The pocket that accommodates the N-terminal side of BH3 α helices displays conformational heterogeneity in the absence of ligand among the viral and cellular proteins. This side of the pocket is formed by α 3 and α 4 and is observed in open, intermediate and closed states (Figure S5). As an example, uncomplexed Bcl-xL adopts a “closed” conformation in the unliganded state, which indeed describes its narrow groove bordered by α 3 and α 4, relative to Bcl-2 (Petros et al., 2001; Petros et al., 2004). However, even uncomplexed Bcl-xL appears to be more “open” at the α 2/ α 5 end of the pocket.

In addition to its recently described role in innate immunity, the biological functions ascribed to DDX3 include RNA splicing, export, and translational regulation (Cullen, 2005; Shih et al., 2008). In contrast to the antagonistic effect of VACV K7, other viruses, including HCV and HIV, have been shown to co-opt DDX3 during infection. The function of DDX3 that is targeted or exploited by viral proteins presumably correlates with their binding sites. The interaction between the nuclear export shuttle protein CRM-1 and DDX3, which is co-opted by the HIV Rev protein, has been roughly mapped to residues 260–517 of DDX3 (Yedavalli et al., 2004). HCV core protein binding maps to the C-terminal region of DDX3 (553–611) (Owsianka and Patel, 1999). In contrast, K7 binds to the N terminus of DDX3, and the effect of DDX3 on innate immune signaling appears to be independent of its RNA helicase function. A DDX3 mutant lacking ATPase activity (K230E) retained its ability to enhance IFN- β induction by TBK1/IKK ϵ (Schroder et al., 2008; Soulat et al., 2008). Furthermore, a DDX3 truncation lacking residues 1–139 was unable to enhance IFN- β promoter induction, suggesting that this function of DDX3 is contained within its N terminus and correlates with the region that is targeted by the viral protein K7 (Schroder et al., 2008).

The structural and functional data presented in this study support a model in which K7 masks a key epitope of DDX3 that is required for the IRF activation pathway via TBK1/IKK ϵ . One possibility is that the diphenylalanine motif interacts directly with IKK ϵ or another effector molecule linking it to the IRF activation pathway. A second hypothesis is that serine/threonine phosphorylation of DDX3 plays a role in downstream activation and that K7 interferes with this process by masking the substrate-binding site. The N terminus of DDX3 is enriched in serine/threonine residues (eight within the segment 71–90) that may be candidates for phosphorylation by IKK ϵ or other protein kinases. These various models can be tested in future mutagenesis and signaling studies. Uncovering the molecular details of interactions between viral

Table 1. Thermodynamics of K7 Interactions with DDX3 Fragments

DDX3 Fragment	K _d (μ M)	Δ H (kcal/mol)	Δ S (cal/mol/deg)
5–167	0.51	–22	–46
5–580	0.46	–30	–72
71–90 ^a	0.93	–26	–61
81–90	1.1	–22	–48
81–100	1.2	–15	–25
71–90 (FF \rightarrow AA)	No binding		

^aSuccessfully crystallized in complex with full-length K7.

immune evasion proteins and their host targets may provide vital information for the design of antivirals and immunosuppressive drugs that mimic the strategy of the virus.

EXPERIMENTAL PROCEDURES

Expression and Purification

Escherichia coli BL21(DE3) cells were transformed with pET15 plasmid harboring a synthetic gene encoding the full-length K7 protein (Genent AG). Liter volume cultures of cells were inoculated with an overnight culture and grown in 2xYT medium (Formedium, UK). Cells were grown to mid-log phase ($OD_{600} = 0.6$) at 310°K, and the culture was cooled in water and ice for a few minutes. Protein expression was subsequently induced by addition of 0.2 mM IPTG (final concentration) with vigorous shaking at 298°K. Following induction for 4–6 hr, cells were harvested by centrifugation and stored frozen if necessary at 250°K.

The expression of selenomethionine-derivitized K7 followed a similar protocol, except that a minimal media (Molecular Dimensions, UK) was used in place of 2xYT. In addition, immediately prior to induction at mid-log phase, the media was supplemented with amino acids Lys, Thr, and Phe (100 mg each); Leu, Ile, and Val (50 mg each); and 50 mg of L(+)-selenomethionine. The cells were suspended in lysis buffer (20 mM Tris-HCl [pH 8.0], 300 mM NaCl, 10 mM imidazole, and 10 mM 2-mercaptoethanol) with a protease inhibitor cocktail (Roche) and were lysed using a Branson sonifier. Following centrifugation at 20,000 g, the soluble fraction was loaded onto a Ni^{2+} -agarose resin equilibrated with lysis buffer. After successive steps of washing with lysis buffer supplemented with up to 30 mM imidazole, K7 was eluted with a step gradient of 200 mM imidazole. The eluted protein was mixed with thrombin (10 units/mg of K7; GE Healthcare) to cleave the His-tag, and was dialyzed against 20 mM Tris-HCl (pH 8.0), 150 mM NaCl, 10 mM imidazole, and 10 mM 2-mercaptoethanol. The dialyzed protein was applied to the Ni^{2+} -agarose resin a second time, and the flow-through fraction contained the cleaved K7 protein.

Further purification involved dialysis into a low-salt buffer (20 mM Tris-Cl [pH 8.0], 20 mM NaCl, and 1 mM dithiothreitol), followed by anion-exchange chromatography with a linear salt gradient to 1 M NaCl. To prepare the K7-DDX3 peptide complex, a two-fold molar excess of peptide was added to the affinity-purified K7 protein, just prior to ion-exchange chromatography. Fractions containing the K7-DDX3 complex were pooled and applied to gel filtration column (Superdex-75, GE Healthcare) equilibrated with 20 mM Tris-HCl (pH 8.0), 150 mM NaCl, and 1 mM DTT. The final purified complex was concentrated and subjected to crystallization procedures. All purification procedures were performed on ice, or at 277°K.

Crystallization and Structure Determination

Initial crystals were grown using the sitting drop vapor diffusion method at 291°K by mixing 100 nl of protein sample at ~10 mg/ml and 100 nl of reservoir solution using a Mosquito robot (TTP Labtech) in 96-well sitting drop plates. Crystals appeared after a few days in 100 mM citrate (pH 5.5), and 20% PEG3350. Final optimized crystals were grown in Linbro 24-well plates using hanging drop vapor diffusion methods with a reservoir solution containing 100 mM sodium citrate (pH 5.25) and 15.0% (w/v) PEG3350. For cryoprotection, the crystals were plunged directly into mother liquor supplemented with 20% (w/v) xylitol. Diffraction data at the selenium peak (0.979 Å) were collected at beamline BM14 at the European Synchrotron Radiation Facility (ESRF) in Grenoble, France. Data were integrated and scaled with DENZO/SCALEPACK package (Otwinowski and Minor, 1997). The structure of the K7-DDX3 peptide complex was solved by SAD methods. Five of six expected selenium sites were found using ShelxD, and density modification was performed using ShelxE (Sheldrick, 2008). The resulting map was readily interpretable, and continuous backbone density of K7 between Tyr7 to Asn149 could be traced with COOT (Emsley and Cowtan, 2004). In parallel, model building was initiated with ArpWarp 7.0.1 (Perrakis et al., 2001), which resulted in automated placement of 272 of 300 residues of K7 (dimer in the asymmetric unit). The remaining K7 residues and the DDX3 peptide were manually built by alternating cycles of model building with COOT (Emsley and Cowtan, 2004) and refinement using Refmac5 (Murshudov et al., 1997). Subsequent iterative model improvement and refinement were performed with COOT and Refmac5. There are two

Table 2. Data Collection and Refinement Statistics

	SeMet (Peak Data)
Data collection	
Space group	C2
Cell dimensions	
a, b, c (Å)	90.89, 69.53, 65.63
α, β, γ (°)	90.00, 122.17, 90.00
Resolution (Å)	30–1.60 (1.66–1.60) ^a
R _{sym}	0.081 (0.373)
I / σ I	35.4 (3.39)
Completeness (%)	97.3 (84.9)
Redundancy	7.0 (4.6)
Shelx D/E phasing	
SeMet sites	5
CC all/weak	47.46/34.15
PATFOM	44.09
Pseudo-free CC	77.92%
Connectivity	0.937
Refinement	
Resolution (Å)	30.0–1.60
No. of reflections	45370 (2267)
R _{work} / R _{free} (%)	14.1/18.9
No. atoms	
K7	2316
DDX3 peptide	160
Water	251
B-factors	
K7 all atoms	17.2
K7 main chain	15.0
K7 side chain	19.4
DDX3 all atoms	19.6
DDX3 main chain	17.8
DDX3 side chain	21.4
Water	28.4
Rmsds	
Bond lengths (Å)	0.0146
Bond angles (°)	1.497

^a Values in parentheses are for highest-resolution shell.

K7-DDX3 complexes in the asymmetric unit, and residues Ser82-Arg88 of DDX3 are well-defined and identical in conformation for both complexes. The rmsd for all atoms in the two complexes is 0.93 Å. The rmsd for K7 atoms is 0.94 Å, whereas the rmsd for equivalent DDX3 peptide atoms is 0.10 Å. However, terminal residues Lys81 and Gly89 of DDX3 are poorly defined and disordered. The sixth SeMet residue was situated in a flexible loop (Met80) in molecule A, thus explaining its poor contribution to the anomalous signal, and was built into the model in later refinement cycles. The initial electron density map from ShelxE is shown together with the final refined model of K7-DDX3 in order to highlight the quality of SAD data (Figure S6). A Ramachandran plot maps 97.9% of residues in the preferred regions, and only one residue (Ser118) lies slightly outside the generous α -helical conformational space. The data and refinement statistics are summarized in Table 2.

Isothermal Titration Calorimetry

Calorimetric measurements were performing using the ITC-200 instrument (MicroCal, Inc). Purified K7 (alone) was dialyzed against 10 mM Tris-Cl

(pH 7.5), 100 mM NaCl, and 1 mM DTT. Following dialysis and concentration of the protein to approximately 60 μ M, the flow-through buffer from the concentrator (iCON, Pierce Inc) was used to directly solubilize the pure peptide (lyophilized powder; EMC Microcollections GmbH) to give a final concentration of 600 μ M. This strategy minimized the buffer mismatch in the subsequent titrations. The same buffer was used to dilute K7 and the DDX3 peptides to obtain ideal concentrations for binding isotherms suitable for subsequent data analyses. Titrations were performed at 293°K with K7 in the reference cell and peptide in the injection cell. The concentrations varied from 250 to 400 μ M for the peptide and from 20 to 50 μ M for K7 protein. For the titration involving the nearly complete fragment of DDX3 (5–580), K7 was loaded into the injection syringe, and DDX3 was placed in the cell. Data analyses by peak integration and curve fitting were performed using the Origin software 7.0, and curves were fit to a single-site binding model to give the binding constant (K_d), enthalpy change (ΔH), and entropy (ΔS) of complex formation.

Mutagenesis and Cellular Studies

The F84A and F85A mutations were simultaneously introduced into the DDX3 sequence by PCR using the previously described pCMV-myc DDX3 construct (Schroder et al., 2008) as a template and Pfu DNA polymerase (New England Biolabs). Coimmunoprecipitations were performed as described elsewhere (Stack et al., 2005). In brief, Ha-tagged K7 and myc-tagged DDX3 or FFAA were cotransfected into HEK293T cells, cells were harvested 48 hr after transfection, and cell lysates were prepared. Antibodies were precoupled to Protein G-Sepharose beads (Sigma) and then were used to immunoprecipitate proteins from cell lysates. Immunocomplexes were analyzed by SDS-PAGE and Western blotting with anti-Ha (Covance) and anti-myc antibodies (Sigma). Promoter induction and transcription factor activation were measured using HEK293 cells seeded onto 96-well plates and were transfected 24 hr later with expression vectors and luciferase reporter genes (Maloney et al., 2005; Schroder et al., 2008; Stack et al., 2005). IRF3 activation was measured using a fusion protein between the DNA-binding domain of the yeast transcription factor GAL4 and IRF3 in conjunction with a GAL4-responsive reporter gene construct. Data are expressed as the mean fold induction \pm SD relative to control levels, for an individual experiment performed in triplicate. A representative of at least three independent experiments is shown.

ACCESSION NUMBERS

The structure of K7-DDX3 peptide has been deposited in the Protein Data Bank with the accession code 3JRV.

SUPPLEMENTAL DATA

Supplemental data include six figures and one movie and may be found with this article online at [http://www.cell.com/structure/supplemental/S0969-2126\(09\)00371-2](http://www.cell.com/structure/supplemental/S0969-2126(09)00371-2).

ACKNOWLEDGMENTS

This study was supported by the Science Foundation Ireland Research Frontiers (grant 08/RFP/BIC980 to A.R.K.) and by the Irish Health Research Board Career Development Fellowship (PD2007/35 to M.S.).

Received: June 29, 2009

Revised: September 10, 2009

Accepted: September 13, 2009

Published: November 10, 2009

REFERENCES

Aoyagi, M., Zhai, D., Jin, C., Aleshin, A., Stec, B., Reed, J., and Liddington, R. (2007). Vaccinia virus N1L protein resembles a B cell lymphoma-2 (Bcl-2) family protein. *Protein Sci.* 16, 118–124.

Ariumi, Y., Kuroki, M., Abe, K., Dansako, H., Ikeda, M., Wakita, T., and Kato, N. (2007). DDX3 DEAD-box RNA helicase is required for hepatitis C virus RNA replication. *J. Virol.* 81, 13922–13926.

Bowie, A., Kiss-Toth, E., Symons, J.A., Smith, G.L., Dower, S.K., and O'Neill, L.A. (2000). A46R and A52R from vaccinia virus are antagonists of host IL-1 and toll-like receptor signaling. *Proc. Natl. Acad. Sci. USA* 97, 10162–10167.

Bowie, A.G., and Unterholzner, L. (2008). Viral evasion and subversion of pattern-recognition receptor signalling. *Nat. Rev. Immunol.* 8, 911–922.

Cooray, S., Bahar, M.W., Abrescia, N.G., McVey, C.E., Bartlett, N.W., Chen, R.A., Stuart, D.I., Grimes, J.M., and Smith, G.L. (2007). Functional and structural studies of the vaccinia virus virulence factor N1 reveal a Bcl-2-like anti-apoptotic protein. *J. Gen. Virol.* 88, 1656–1666.

Cullen, B.R. (2005). Human immunodeficiency virus: nuclear RNA export unwound. *Nature* 433, 26–27.

Day, C.L., Chen, L., Richardson, S.J., Harrison, P.J., Huang, D.C., and Hinds, M.G. (2005). Solution structure of pro-survival Mcl-1 and characterization of its binding by proapoptotic BH3-only ligands. *J. Biol. Chem.* 280, 4738–4744.

Day, C.L., Smits, C., Fan, F.C., Lee, E.F., Fairlie, W.D., and Hinds, M.G. (2008). Structure of the BH3 domains from the p53-inducible BH3-only proteins Noxa and Puma in complex with Mcl-1. *J. Mol. Biol.* 380, 958–971.

Emsley, P., and Cowtan, K. (2004). Coot: model-building tools for molecular graphics. *Acta Crystallogr. D Biol. Crystallogr.* 60, 2126–2132.

Graham, S.C., Bahar, M.W., Cooray, S., Chen, R.A., Whalen, D.M., Abrescia, N.G., Alderton, D., Owens, R.J., Stuart, D.I., Smith, G.L., and Grimes, J.M. (2008). Vaccinia virus proteins A52 and B14 share a Bcl-2-like fold but have evolved to inhibit NF- κ B rather than apoptosis. *PLoS Pathog.* 4, e1000128.

Harte, M.T., Haga, I.R., Maloney, G., Gray, P., Reading, P.C., Bartlett, N.W., Smith, G.L., Bowie, A., and O'Neill, L.A. (2003). The poxvirus protein A52R targets Toll-like receptor signaling complexes to suppress host defense. *J. Exp. Med.* 197, 343–351.

Hogbom, M., Collins, R., van den Berg, S., Jenvert, R.M., Karlberg, T., Kotenyova, T., Flores, A., Hedestam, G.B., and Schiavone, L.H. (2007). Crystal structure of conserved domains 1 and 2 of the human DEAD-box helicase DDX3 in complex with the mononucleotide AMP. *J. Mol. Biol.* 372, 150–159.

Kalverda, A.P., Thompson, G.S., Vogel, A., Schroder, M., Bowie, A.G., Khan, A.R., and Homans, S.W. (2009). Poxvirus K7 protein adopts a Bcl-2 fold: biochemical mapping of its interactions with human DEAD box RNA helicase DDX3. *J. Mol. Biol.* 385, 843–853.

Keating, S.E., Maloney, G.M., Moran, E.M., and Bowie, A.G. (2007). IRAK-2 participates in multiple toll-like receptor signaling pathways to NF κ B via activation of TRAF6 ubiquitination. *J. Biol. Chem.* 282, 33435–33443.

Kvansakul, M., van Delft, M.F., Lee, E.F., Gulbis, J.M., Fairlie, W.D., Huang, D.C., and Colman, P.M. (2007). A structural viral mimic of pro-survival Bcl-2: a pivotal role for sequestering proapoptotic Bax and Bak. *Mol. Cell* 25, 933–942.

Kwong, A.D., Rao, B.G., and Jeang, K.T. (2005). Viral and cellular RNA helicases as antiviral targets. *Nat. Rev. Drug Discov.* 4, 845–853.

Lardone, M.C., Parodi, D.A., Valdevenito, R., Ebensperger, M., Piottante, A., Madariaga, M., Smith, R., Pommer, R., Zambrano, N., and Castro, A. (2007). Quantification of DDX3Y, RBMY1, DAZ and TSPY mRNAs in testes of patients with severe impairment of spermatogenesis. *Mol. Hum. Reprod.* 13, 705–712.

Liu, X., Dai, S., Zhu, Y., Marrack, P., and Kappler, J. (2003a). The structure of a Bcl-xL/Bim fragment complex: Implications for Bim function. *Immunity* 19, 341–352.

Liu, X., Dai, S., Zhu, Y., Marrack, P., and Kappler, J.W. (2003b). The structure of a Bcl-xL/Bim fragment complex: implications for Bim function. *Immunity* 19, 341–352.

Maloney, G., Schroder, M., and Bowie, A.G. (2005). Vaccinia virus protein A52R activates p38 mitogen-activated protein kinase and potentiates lipopolysaccharide-induced interleukin-10. *J. Biol. Chem.* 280, 30838–30844.

McCoy, S.L., Kurtz, S.E., MacArthur, C.J., Trune, D.R., and Hefeneider, S.H. (2005). Identification of a peptide derived from vaccinia virus A52R protein that inhibits cytokine secretion in response to TLR-dependent signaling and reduces in vivo bacterial-induced inflammation. *J. Immunol.* 174, 3006–3014.

Moynagh, P.N. (2005). The NF- κ B pathway. *J. Cell Sci.* 118, 4589–4592.

- Murshudov, G.N., Vagin, A.A., and Dodson, E.J. (1997). Refinement of macromolecular structures by the maximum-likelihood method. *Acta Crystallogr. D Biol. Crystallogr.* 53, 240–255.
- O'Neill, L.A. (2006). Translational mini-review series on Toll-like receptors: recent advances in understanding the role of Toll-like receptors in anti-viral immunity. *Curr. Opin. Immunol.* 18, 3–9.
- Otwinowski, Z., and Minor, W. (1997). Processing of X-ray diffraction data collected in oscillation mode. *Methods Enzymol.* 276, 307–326.
- Owsianka, A.M., and Patel, A.H. (1999). Hepatitis C virus core protein interacts with a human DEAD box protein DDX3. *Virology* 257, 330–340.
- Perrakis, A., Harkiolaki, M., Wilson, K.S., and Lamzin, V.S. (2001). ARP/wARP and molecular replacement. *Acta Crystallogr. D Biol. Crystallogr.* 57, 1445–1450.
- Petros, A.M., Medek, A., Nettesheim, D.G., Kim, D.H., Yoon, H.S., Swift, K., Matayoshi, E.D., Oltersdorf, T., and Fesik, S.W. (2001). Solution structure of the antiapoptotic protein Bcl-2. *Proc. Natl. Acad. Sci. USA* 98, 3012–3017.
- Petros, A.M., Olejniczak, E.T., and Fesik, S.W. (2004). Structural biology of the Bcl-2 family of proteins. *Biochim. Biophys. Acta* 1644, 83–94.
- Rosner, A., and Rinkevich, B. (2007). The DDX3 subfamily of the DEAD box helicases: divergent roles as unveiled by studying different organisms and in vitro assays. *Curr. Med. Chem.* 14, 2517–2525.
- Sattler, M., Liang, H., Nettesheim, D., Meadows, R., Harlan, J., Eberstadt, M., Yoon, H., Shuker, S., Chang, B., Minn, A., et al. (1997). Structure of Bcl-xL–Bak peptide complex: recognition between regulators of apoptosis. *Science* 275, 983–986.
- Schroder, M., Baran, M., and Bowie, A.G. (2008). Viral targeting of DEAD box protein 3 reveals its role in TBK1/IKKepsilon-mediated IRF activation. *EMBO J.* 27, 2147–2157.
- Sengoku, T., Nureki, O., Nakamura, A., Kobayashi, S., and Yokoyama, S. (2006). Structural basis for RNA unwinding by the DEAD-box protein *Drosophila* Vasa. *Cell* 125, 287–300.
- Sheldrick, G.M. (2008). A short history of SHELX. *Acta Crystallogr. A* 64, 112–122.
- Shih, J.W., Tsai, T.Y., Chao, C.H., and Wu Lee, Y.H. (2008). Candidate tumor suppressor DDX3 RNA helicase specifically represses cap-dependent translation by acting as an eIF4E inhibitory protein. *Oncogene* 27, 700–714.
- Smith, G.L., Chan, Y.S., and Howard, S.T. (1991). Nucleotide sequence of 42 kbp of vaccinia virus strain WR from near the right inverted terminal repeat. *J. Gen. Virol.* 72, 1349–1376.
- Soulat, D., Burckstummer, T., Westermayer, S., Goncalves, A., Bauch, A., Stefanovic, A., Hantschel, O., Bennett, K.L., Decker, T., and Superti-Furga, G. (2008). The DEAD-box helicase DDX3X is a critical component of the TANK-binding kinase 1-dependent innate immune response. *EMBO J.* 27, 2135–2146.
- Stack, J., Haga, I., Schroder, M., Bartlett, N., Maloney, G., Reading, P., Fitzgerald, K., Smith, G., and Bowie, A. (2005). Vaccinia virus protein A46R targets multiple Toll-like-interleukin-1 receptor adaptors and contributes to virulence. *J. Exp. Med.* 201, 1007–1018.
- Takaoka, A., and Taniguchi, T. (2008). Cytosolic DNA recognition for triggering innate immune responses. *Adv. Drug Deliv. Rev.* 60, 847–857.
- Wang, H., Kim, S., and Ryu, W.S. (2009). DDX3 DEAD-Box RNA helicase inhibits hepatitis B virus reverse transcription by incorporation into nucleocapsids. *J. Virol.* 83, 5815–5824.
- Yedavalli, V.S.R.K., Neuveut, C., Chi, Y.H., Kleiman, L., and Jeang, K.T. (2004). Requirement of DDX3 DEAD box RNA helicase for HIV-1 REV-RRE export function. *Cell* 119, 381–392.